JOURNAL OF MATERIALS SCIENCE **36** (2001) 1963–1973

Implantation parameters affecting aluminum nano-particle formation in alumina

E. M. HUNT
Columbian Chemicals Company, Marietta, GA 30062-2253, USA

J. M. HAMPIKIAN
School of Materials Science and Engineering, Georgia Institute of Technology, Atlanta, GA 30332-0245, USA
E-mail: janet.hampikian@mse.gatech.edu

The formation of nano-dimensional metallic Al precipitates in alumina due to the reduction of the host matrix as a result of ambient temperature ion implantation of Y ions is examined. The formation and growth of Al precipitates are dependent on both the Y ion dose and the energy available to the matrix, as reported here. Reducing the ion dose from 5×10^{16} to 2.5×10^{16} ions/cm^2 results in smaller precipitates; 10.7 ± 1.8 nm to 9.0 nm ± 1.2 nm, respectively, for incident ion energies of 150 keV, based upon particle size measurements obtained using energy filtered transmission electron microscopy. Below a fluence of 2.5×10^{16}, particle formation is not detected. The energy available to the matrix was varied; first, by controlling the incident ion energy (varied between 60 and 150 keV) while holding the substrate at ambient temperature, and second, by controlling the substrate temperature (varied between 44 and 873 K) while holding the incident ion energy constant at 150 keV. Experiments conducted with incident ion energies of 110 keV or higher produce crystalline Al precipitates; whereas implantations at 100 keV produce amorphous Al particles and implantations at 60 keV produce no detectable precipitates. The implantations carried out as a function of temperature produce successively smaller precipitates with decreasing temperature to 77 K (6.7 ± 1.0 nm), below which no precipitates are detected. An Arrhenius activation energy for the formation of the aluminum precipitates of 1.7 kJ/mole has been calculated using the volume of precipitates formed as a function of inverse temperature. This low activation energy suggests that radiation enhanced diffusion (RED) is responsible for particle growth during these implantations. © *2001 Kluwer Academic Publishers*

1. Introduction
1.1. Motivation
Dielectric materials with unusual optical properties have a wide variety of possible applications which range from photoluminescent silica substrates to transparent dielectrics with nonlinear optical responses such as an intensity-dependent index of refraction. The former are interesting because of their high efficiency at room temperatures and the latter are promising candidates for applications in the area of optical waveguide technology [1–4]. These two examples are similar in that the desirable properties are the result of a fine dispersion of nano-sized ($<\sim$15 nm) metallic or semiconducting particles embedded in a dielectric substrate. Ion implantation is one of several techniques which readily lends itself to the configuration and fabrication requirements of these types of devices. Hence, nanoparticle formation in dielectric materials via ion implantation has been a technique that has been studied intensively in the recent past.

1.2. Implantation as a particle-forming mechanism in alumina
Ion implantation provides a mechanism with which to introduce a relatively large local concentration of an element into a substrate at some depth beneath the surface. If the implanted element has a low solubility limit in the substrate material it is not energetically favorable for the element to remain in solution. In this situation precipitation and/or chemical reaction will take place if the energy barriers to those processes can be overcome with the available thermodynamic and kinetic energy. This process of implanted ion precipitation has been extensively studied in aluminum oxide substrates.

There are only a few elements that will form nanoparticles in alumina as a result of ion implantation alone. Those elements include Ag [5] and Nb [6] implanted to fluences in the 10^{16} ions/cm^2 range. Metallic nanoparticles of Fe [7, 8] will also form in alumina during implantation if the iron is implanted to fluences of 10^{17} ions/cm^2 or greater. Ion

implantation of $\sim 10^{16}$ Au [9], Si or Ge [10] ions/cm^2 carried out with the substrate held at elevated temperatures will also cause precipitation and particle formation. The heat introduced to the substrate during implantation provides the energy required for precipitation of the implanted element. Post-implantation heat treatment is another way to introduce extra energy into an implanted system and is sometimes required for precipitation and particle formation in alumina.

1.3. Previous research

Previous research [11, 12] has shown that ion implantation of yttrium into [02 01] [0 2 $\bar{2}$ 1] sapphire, to a dose of 5×10^{16} Y^+/cm^2, administered at energies between 100 and 150 keV and at ambient temperature, will produce metallic aluminum nanoparticles in alumina in agreement with the predictions of equilibrium thermodynamic principles. These nanoparticles were shown to have a lattice parameter of 0.412 nm ± .002 nm, and an average particle size 12.5 nm. This lattice parameter is close to that of pure, metallic Al (0.404 nm). Electron energy loss spectroscopy (PEELS) was used to demonstrate the metallic nature of the Al found in these particles by allowing the examination of the low loss (0–40 eV) region of the electron energy loss spectrum which may be used to differentiate metallic and oxidized Al. Energy filtered transmission electron microscopy (EFTEM) further confirmed the presence of metallic Al in the particles themselves by allowing electron images to be formed using only electrons that have experienced the energy loss characteristic of metallic Al.

The mechanism of formation of these Al particles does not appear to be supersaturation and precipitation which is the most common mechanism for the formation of metallic particles in an oxide matrix as described in Section 1.2, in which ion implanted elements form particles comprised of the implanted ion. The substrates in this study, in contrast, are implanted with Y and the resulting particles are comprised of Al. Lattice dissociation and the formation of particles from the cation of the host lattice have been reported previously [13–19]; however, in these cases the matrix material was irradiated with high energy (MeV range) electron or neutrons. The matrix material in this study was implanted with relatively low energy ions. Therefore, the mechanism of lattice dissociation due to high energy irradiation does not appear to be active either. The mechanism for the production of free metallic aluminum is the reduction of the alumina substrate by the implanted yttrium ions, [12, 20] via

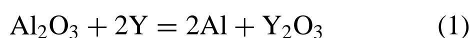

$$Al_2O_3 + 2Y = 2Al + Y_2O_3 \quad (1)$$

The Gibbs free energy values for the free energy of this reaction over the range of temperatures appropriate to these experiments are negative, indicating that this reaction is thermodynamically possible. Conversely, a similar calculation for a different implant ion yields positive free energies for many of the implantations done by other researchers who did not report the formation of aluminum particles following ion implantation of various elements in Al_2O_3, including Ni, Mn, Ge, Ag, Cu, Fe, and Si. The lack of Al particle formation in these cases is thus consistent with this mechanism of particle formation via reduction.

2. Experimental

The sapphire substrates used in this research were donated by Saphikon Inc. and have been experimentally determined to be [0 2 $\bar{2}$ 1] in orientation. The 10 cm × 10 cm × 0.72 mm optically polished substrates were cut into 1 cm × 1 cm pieces using a slow speed diamond saw. The samples were annealed at 1500 °C for 80 hours to remove residual polishing damage and ensure a crystalline structure throughout the substrate. The crystallinity of the substrate surface was verified by electron channeling in a scanning electron microscope (SEM) using a backscattered electron detector and 10 keV electrons [11].

The initial implantations of singly charged Y ions (Y^+) were performed with an ion implanter coupled with a high vacuum end station. The pressure during implantation was maintained at $\approx 5 \times 10^{-6}$ Pa. The latter implantations of Y^+ and all other ions were conducted in the Surface Modification and Characterization Facility in the Solid State Division of Oak Ridge National Laboratory. The vacuum was held in the range of 10^{-4} Pa and the implantation was carried out in an Extrion ion implanter utilizing the Freeman ion source configuration. The accelerating potential ranged between 60 and 150 keV, and yielded singly charged ions at those energies.

Examination of as-implanted substrates was carried out using TEM, energy dispersive spectrometry (EDS), PEELS and EFTEM. TEM, EDS and PEELS experiments were carried out at the Georgia Institute of Technology using a field emission gun transmission electron microscope operated at 200 keV with a typical operating intensity of 16–20 μA. The particle measurements from bright field TEM images are reported, in accordance with the literature, as a particle size range with an average size and associated standard deviation. This TEM is also equipped with a 576 pixel × 384 pixel CCD camera, a light element EDS detector and a parallel detection electron energy loss spectrometer with a variable size entrance aperture.

The optical absorption measurements were recorded using either a Lambda-9 or a Cary 500 dual beam spectrophotometer. The absorption presented here is labeled "Relative Absorbance" and was collected with an unaltered sample of the substrate material in the reference beam, resulting in a plot of differential, or normalized absorption. The relative absorbance is plotted with a dimensionless ordinate with a maximum of approximately unity.

EFTEM makes it possible to perform chemically sensitive imaging using electrons which have experienced the inelastic energy losses associated with passing through a thin foil TEM sample. Each element causes electrons that have interacted with it to experience a characteristic set of energy losses. This energy

loss spectrum provides a fingerprint of the elements present in the sample. In some cases this type of spectroscopy can also differentiate between different oxidation states. By separating the electrons with different energy losses at the exit face of the electron energy-loss spectrometer, introducing an energy selecting system that allows only electrons with a specified loss to pass through the system, and finally redispersing those allowed electrons with a set of magnetic lenses in correspondence with their real space distribution, a chemically sensitive image may be formed. In this work the plasmon or valence region of the spectrum is used to differentiate between oxidized and metallic Al. This region is considered the low-loss region and extends from 0 to ∼40 eV loss. In a few cases images were formed using electrons with a larger energy loss characteristic of a core electron interaction. The EFTEM experiments were carried out at Oak Ridge National Laboratory in the Metals and Ceramics Division's Radiation Effects and Microstructural Analysis Group (REMAG) using a Gatan Imaging Filter (GIF^{TM}) interfaced to a Philips CM30 TEM operated at 300 kV. All energy-loss images were 512 × 512 pixels in size and were gain normalized to eliminate any artifacts resulting from variation in the electrical response of the pixels of the CCD. The low-loss images were recorded with an exposure time of ∼1 second and an energy-selecting window of 5 eV. Images acquired using core-loss electrons were recorded with an exposure time of 30 seconds and an energy-selecting window of 30 eV. Further detail is given elsewhere (11, 21–23).

3. Results

The preliminary work presented in the introduction raises a number of issues regarding the formation of metallic Al particles in alumina. The experiments reported here investigate the processes involved in the evolution of Al particle formation in alumina during implantation. Two critical factors expected to affect particle formation include the energy available to the free Al atoms which form via reduction and the concentration of those ions in the region of particle formation. These variables must be indirectly investigated by manipulating the implantation parameters that are known to affect particle formation in other systems, namely, ion fluence, incident ion energy and implantation temperature.

3.1. Ion fluence series

Altering the ion fluence, or number of ions per unit area incident on the sample will affect the maximum concentration of ions at the peak of the implantation profile. All previous experiments have involved the implantation of 5×10^{16} ions/cm^2. The effects of reducing this fluence to 4, 2.5 and 1×10^{16} Y^+ ions/cm^2 at 150 keV are now presented. All other implantation parameters, such as temperature and current density have been held constant. The free Al concentration is expected to scale with the concentration of the Y^+ at the peak of the concentration profile, which is predicted to change

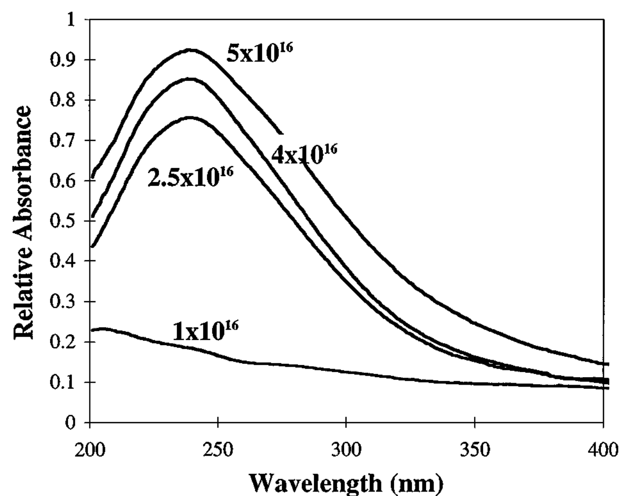

Figure 1 Relative optical absorption spectra from the incident ion fluence series of Y^+-implantations into alumina showing the slight intensity differences between the implantation of various fluences and the lack of a similar absorption feature in the low fluence implant.

from 7.4 to 2.3 at % for fluences of 5×10^{16} and 1×10^{16} Y^+/cm^2, respectively [24].

Optical absorption spectra for this series of implanted substrates are shown in Fig. 1. The three largest fluence implants exhibit strong absorption features at 240 nm, while the 1×10^{16} ions/cm^2 implantation shows no evidence of an absorption feature indicative of the presence of nanoparticles. The most striking distinction between these spectra is the difference in absorption feature intensity, with the higher fluence implants having absorption peaks with greater intensity. These spectra have been normalized to the spectrum with the lowest relative absorption value at 800 nm.

TEM examination via imaging and electron diffraction of this series of implantations shows that only the substrates which demonstrate an absorption peak contain crystalline metallic Al particles as seen pictorially in Fig. 2. The particles range in size from 7–14 nm with average sizes of 9.0 nm ± 1.2 nm and 10.7 nm ± 1.8 nm for the 2.5 and 5×10^{16} ions/cm^2 implants respectively. The substrate implanted with the smallest fluence shows no diffraction evidence suggestive of particles. EFTEM experiments carried out on this sample also show no indication of diffraction or compositional contrast of any kind, indicating that this sample does

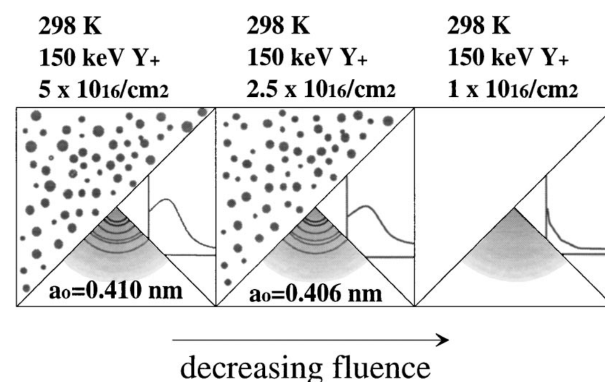

Figure 2 Graphical summary of the incident ion fluence series of Y^+-implantations into alumina.

not contain any detectable type of metallic Al clusters. The lack of particle formation in the low-end implant suggests that there is a lower limit to the concentration at which the implantation of yttrium into alumina will result in Al particle formation. This lower limit would appear to occur between approximately 2.3 at % and 5.1 at %, the predicted peak concentration profiles [24] corresponding to 1×10^{16} and 2.5×10^{16} Y^+/cm^2, respecively.

3.2. Incident ion energy series

When surface sputtering considerations are taken into account a change in the accelerating energy of the incident ions will only marginally affect the concentration of implanted ions at the peak of the ion profile while radically altering the energy available for ion/lattice interactions [24]. Thus it is possible to vary the incident ion energy while holding the peak implanted ion concentration approximately constant. The incident ion energy may be critical to the formation of the Al particles which result from the implantation of Y^+ into alumina. A series of implantations has been performed in which all other implantation parameters (fluence, current density, temperature, ion, substrate) were held constant while the incident ion energy was reduced from 150 keV, an energy known to produce crystalline particles, to 130,110, 100 and 60 keV. The Al clusters formed during implantation at 150, 130 and 110 keV were crystalline (Fig. 3) while those formed during the 100 keV implant were noncrystalline [23]. The sample implanted at 60 keV did not demonstrate any particle formation. This information is summarized pictorially on the vertical axis of Fig. 4.

The differential optical absorption spectra for this series of implantations are shown in Fig. 5. The 150, 130 and 110 keV implantations demonstrate absorption features at 240 nm, 240 nm and 242 nm, respectively. The 60 and 100 keV implanted substrates exhibit no obvious absorption features indicative of crystalline nanoscale particles. The higher energy implants result in absorption peaks of greater intensity. These spectra have been normalized to the level of the spectrum with the lowest absorption value at 800 nm in order to eliminate the "background" absorption due to the increased coloration of the substrates implanted at high energies.

TEM analysis of the implanted substrates in this series reveals crystalline metallic Al particles present in the 150, 130 and 110 keV implanted substrates. These samples show absorption features near 240 nm.

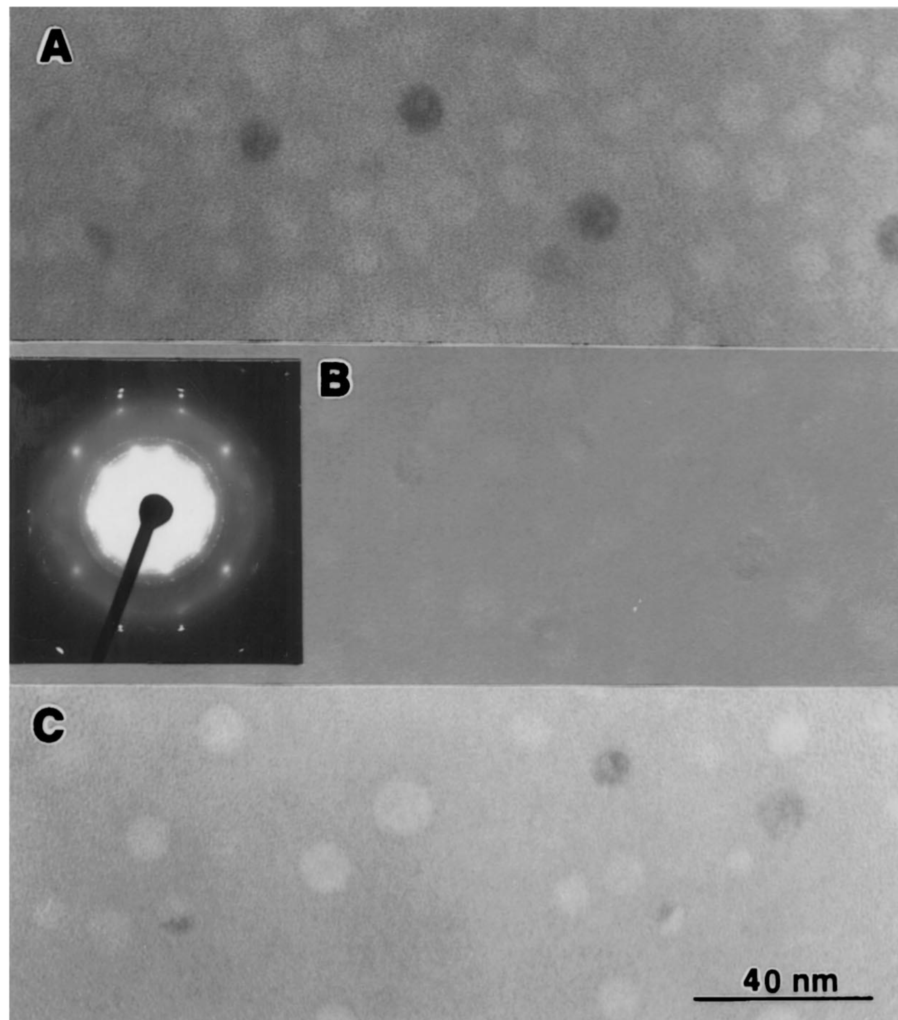

Figure 3 Bright field TEM images of the particle-bearing members of the incident ion energy series of implantations showing a slight particle size decrease with decreasing energy. A) 150 keV Y^+-implant, B) 130 keV Y^+-implant, C) 110 keV Y^+-implant. Inset in B) shows diffraction pattern from implanted region in B); diffraction rings result from the particles produced from implantation; main spots result from the single crystal substrate.

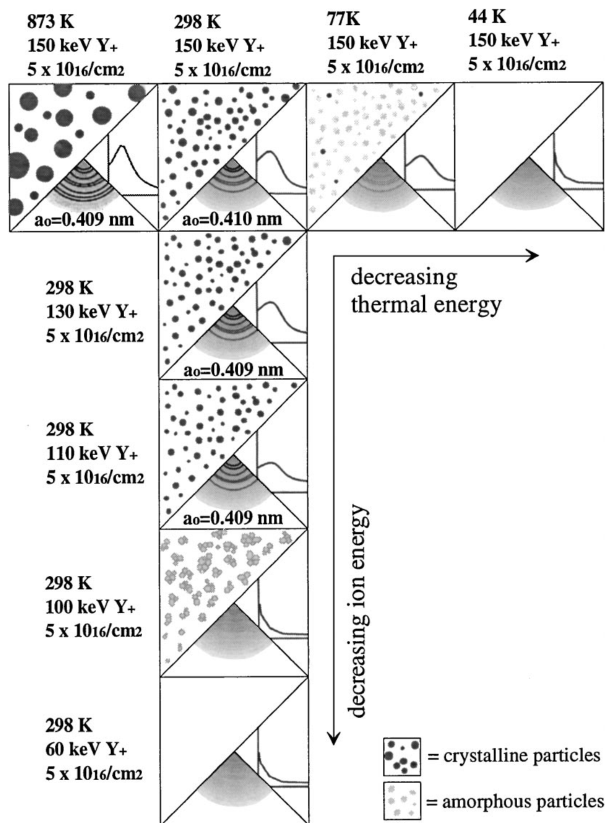

Figure 4 Graphical summary of the results of the implanted ion energy and controlled temperature series of Y^+-implantations into alumina.

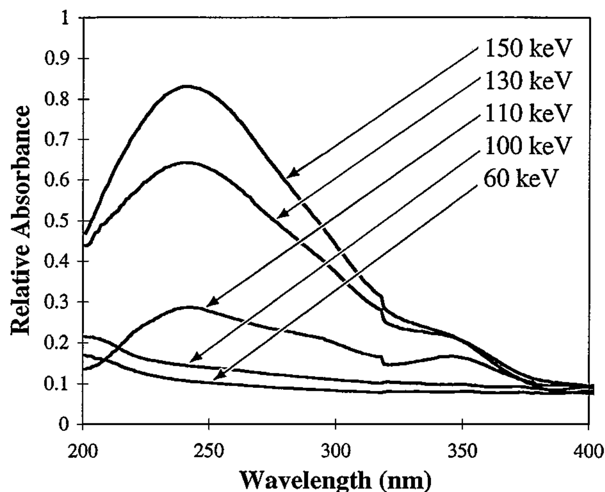

Figure 5 Relative optical absorption spectra from the incident ion energy series of Y^+-implantations into alumina showing the presence of absorption features for the 150, 130, 120 and 110 keV implantations and the lack of similar absorption features for the 100 and 60 keV implantations.

The particle sizes varied slightly with implant energy, yielding particles with average sizes of 10.7 nm ± 1.8 nm, 10.5 nm ± 1.9 nm and 9.0 nm ± 1.6 nm for the 150, 130 and 110 keV implanted substrates, respectively. In all cases the implanted substrate material was amorphous, consistent with the microhardness measurements. Since the lower energy implantations did not produce particles although their microhardnesses indicated an amorphous surface layer it appears that the formation of such a layer is not necessarily a result of, or responsible for the reduction of the substrate.

3.3. Implantation temperature series

The total energy available in the substrate at a given current density to both the implanted ions and the free Al atoms can be influenced by controlling the available thermal energy. The previously presented implantations were carried out with the substrate attached to the sample implantation block with conductive paint. This configuration allows some of the beam-generated heat to be transferred to the sample block; however, there was a small amount of beam heating of the substrate. This beam heating was kept to a minimum by keeping the beam current density low, in the 1–3 μA range. In the following series of experiments, the substrate temperature was varied by actively heating or cooling the sample block during implantation. Four different implantation temperatures were investigated; 873 K, 298 K, 77 K and 44 K. All other implantation conditions were kept constant, with the implantation of a 150 keV low current density beam of 5×10^{16} Y^+ ions/cm^2.

The differential optical absorption measurements resulting from these substrates are presented in Fig. 6. The dramatic difference in the absorption features indicates immediately that there is a large difference in the particle morphology of the four substrates. The high temperature implantation exhibits an intense, sharp absorption peak at 240 nm, while the liquid nitrogen temperature implant (77 K) exhibits a weaker, much broader absorption peak at 258 nm. The lowest temperature implant carried out at 44 K exhibits no obvious absorption feature at all.

TEM examination of these substrates shows that the 873 K implant contains large, spherical particles ranging in size from 22–43 nm with an average size of 34 nm ± 5 nm, see Fig. 7a. These particles possess a polycrystalline diffraction pattern that identifies them as metallic aluminum with a lattice parameter of 0.409 nm ± 0.002 nm. As described earlier, the 298 K sample contains metallic aluminum particles with an average size of 10.7 ± 1.8 nm, Fig. 7b. The 77 K (−196 °C) temperature implanted substrate contains

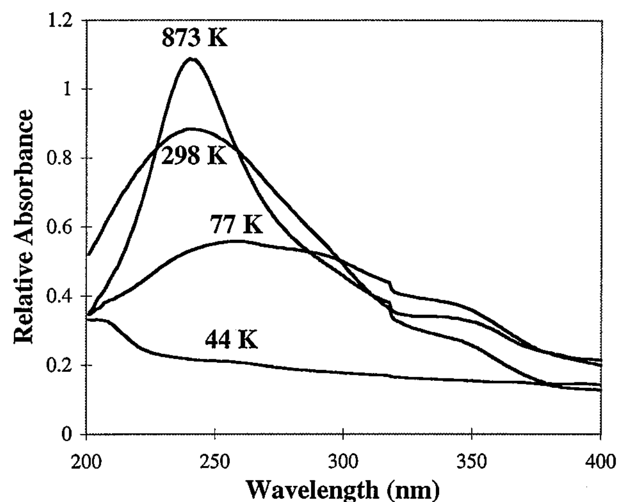

Figure 6 Relative optical absorption spectra from the temperature controlled series of Y^+-implantations into alumina showing the intensity differences between implantations carried out at varying temperatures and the lack of a similar absorption feature in the lowest temperature implant.

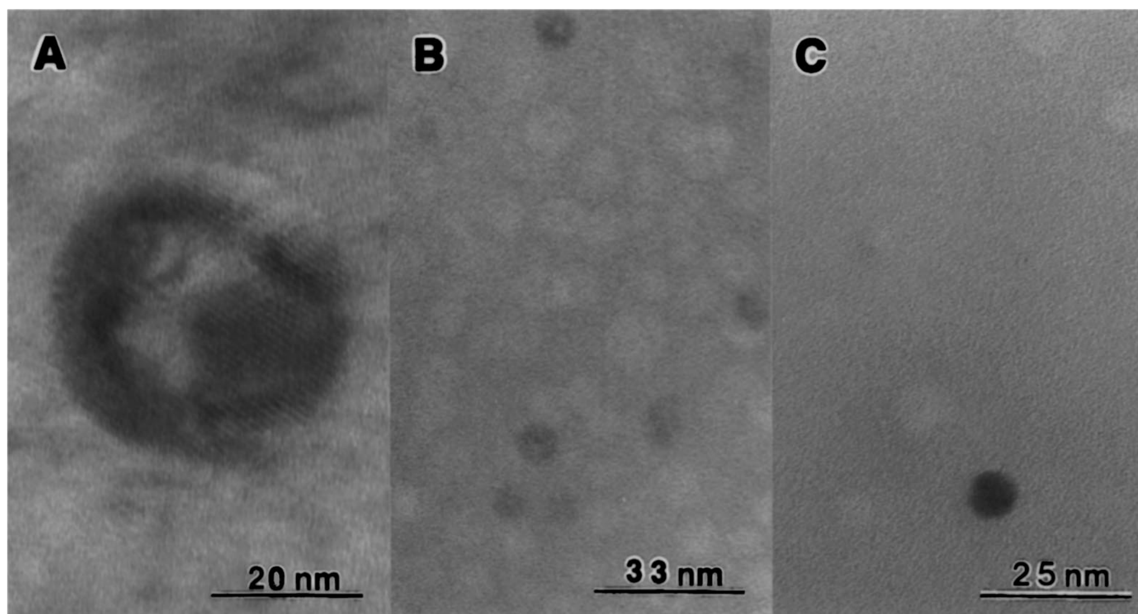

Figure 7 Bright field TEM of the A) 873 K, B) 298 K and C) 77 K Y^+-implants into alumina.

very few crystalline particles which range in size from 5–8 nm with an average size of 6.7 nm ± 1.0 nm, see Fig. 8c. There are so few of these contained in the large amorphous region of this substrate that no polycrystalline pattern can be detected, despite the obvious diffraction contrast that makes the particles visible. The lowest temperature implantation (44 K) does not appear to contain any features demonstrating diffraction contrast when examined with TEM (not shown).

PEELS and EFTEM experiments both confirm that the particles present in the 873 K implantation are metallic aluminum. Fig. 8 shows a series of energy filtered images at 15, 25 and 40 eV loss used to confirm the particles' identity as metallic Al. The use of PEELS and EFTEM to identify the metallic Al phase is presented elsewhere [21–23] and for brevity will not be discussed in detail here. EFTEM on the 77 K implant reveals quite a different picture of this sample than was seen in conventional TEM. Fig. 9 shows an EFTEM series of images which reveals that the particles are Al and that the density of particles is greater than the TEM analysis indicates (see Figs 7c and 9). The particles that appear in the 15 eV loss image (Fig. 9) and which do not appear in conventional bright field (Figs 7c and 9) are assumed to be amorphous as they exhibit no diffraction contrast. The particles in the EFTEM image have a size range of 7–12 nm ± the 2 nm resolution expected from a 15 eV-loss plasmon image. Both PEELS and EFTEM of the lowest temperature implantation (44 K) reveal a lack of any type of signal or contrast indicative of the presence of aluminum particles in the examined portion of the TEM thin foil. This null-result, in conjunction with the lack of diffraction contrast and diffraction pattern seen in TEM and the lack of an optical absorption peak all lead to the conclusion that the substrate implanted at 44 K did not experience any measurable Al particle formation.

3.4. Calculated volume fraction of metallic aluminum

In order to further investigate the feasibility of the idea that the Al particle formation is the result of ion implantation-induced reduction, the total experimental volume fraction of Al present in the implanted substrates (VF_{ED}) is calculated in this section and compared with the volume fraction of metallic Al that is theoretically possible (VF_T), assuming that each incident ion produces one Al atom via reduction of the substrate. It should not be possible for the ratio of these volume fractions ($R = VF_{ED}/VF_T$) to exceed unity within the framework of the proposed mechanism.

This ratio (R) may be calculated using particle size measurements from EFTEM images and certain parameters of the ion implantation as determined by PROFILE [24]:

$$R = \frac{VF_{EP}}{VF_T} = \frac{\left[\dfrac{\sum_{i=1}^{b}\left(\frac{4}{3}\pi Ri^3\right)Ni}{R_P(\text{area})}\right]}{\dfrac{\text{Dose}_R/\text{Density}_{Al}}{R_P}} \tag{3}$$

where the theoretical upper limit of the Al volume fraction (VF_T) is found using the retained dose (Dose_R), the density of metallic Al (Density_{Al}) and the total implanted volume ($1\ \text{cm}^2$). The experimentally determined volume fraction of Al (VF_{ED}) is found by summing the volumes of the particles measured in an EFTEM image and dividing by the implanted volume in each measured area (R_P and Area). In this equation, the summation of the particle volume is accomplished in a distributed manner by defining Ri as the radius of the ith bin, Ni as the number of particles whos radium

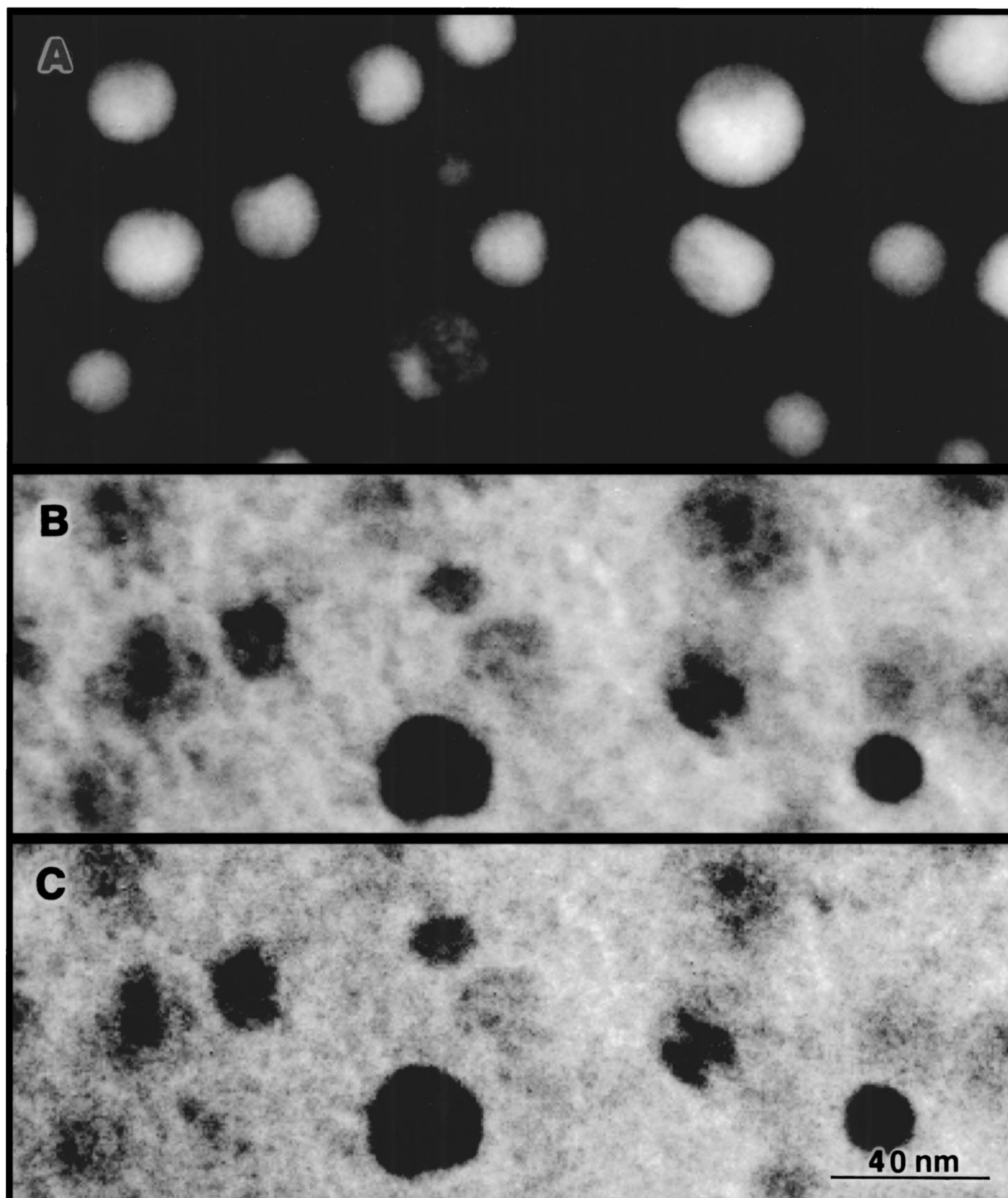

Figure 8 Series of EFTEM images from the 873 K Y^+-implant into alumina. Image A) is a 15 eV-loss image, B) is a 25 eV-loss image and C) is a 40 eV-loss image.

lies within the radium range of the ith sorting bin and b as the number of 2 nm bins required to sort the particle sizes. The 15 eV-loss images were used for these measurements because of the high contrast and higher particle density visible in the EFTEM images.

This method of volume fraction calculation is found to yield values that lie between the volume fractions calculated using the simple average particle diameters measured from TEM and those measured from EFTEM images [25]. The "distributed" volume fractions VF_{ED} reported here are used for further discussion.

A number of assumptions were made in these calculations. First, it is assumed that the particles reside in a layer of material with a thickness equal to the range of the original implantation (R_p). It is further assumed that the whole volume of this implanted material is contained within the TEM thin foil pictured in the measured image area. Considering that most TEM foils are at least 100 nm in thickness and that the largest projected range in these experiments is ~50 nm, this appears to be a reasonable assumption. Should the particles reside in a larger region, the volume of implanted material would be underestimated resulting in a volume fraction that errs toward a larger percentage. Conversely, if the particles reside in a smaller volume, the volume fraction values would be artificially low.

An additional assumption concerns the form of the particles themselves. The particles are considered to be spherical in shape and composed of fully dense Al. Shape variations could cause volume calculation errors; however, for most of these substrates the particles appear generally spherical. All particles in a designated area of the EFTEM image were measured.

The values for the experimentally determined and the theoretical maximum volume fractions for the implanted substrates are compared in Table I. The first important trend to note is that all of the experimental volume fractions are significantly lower than the

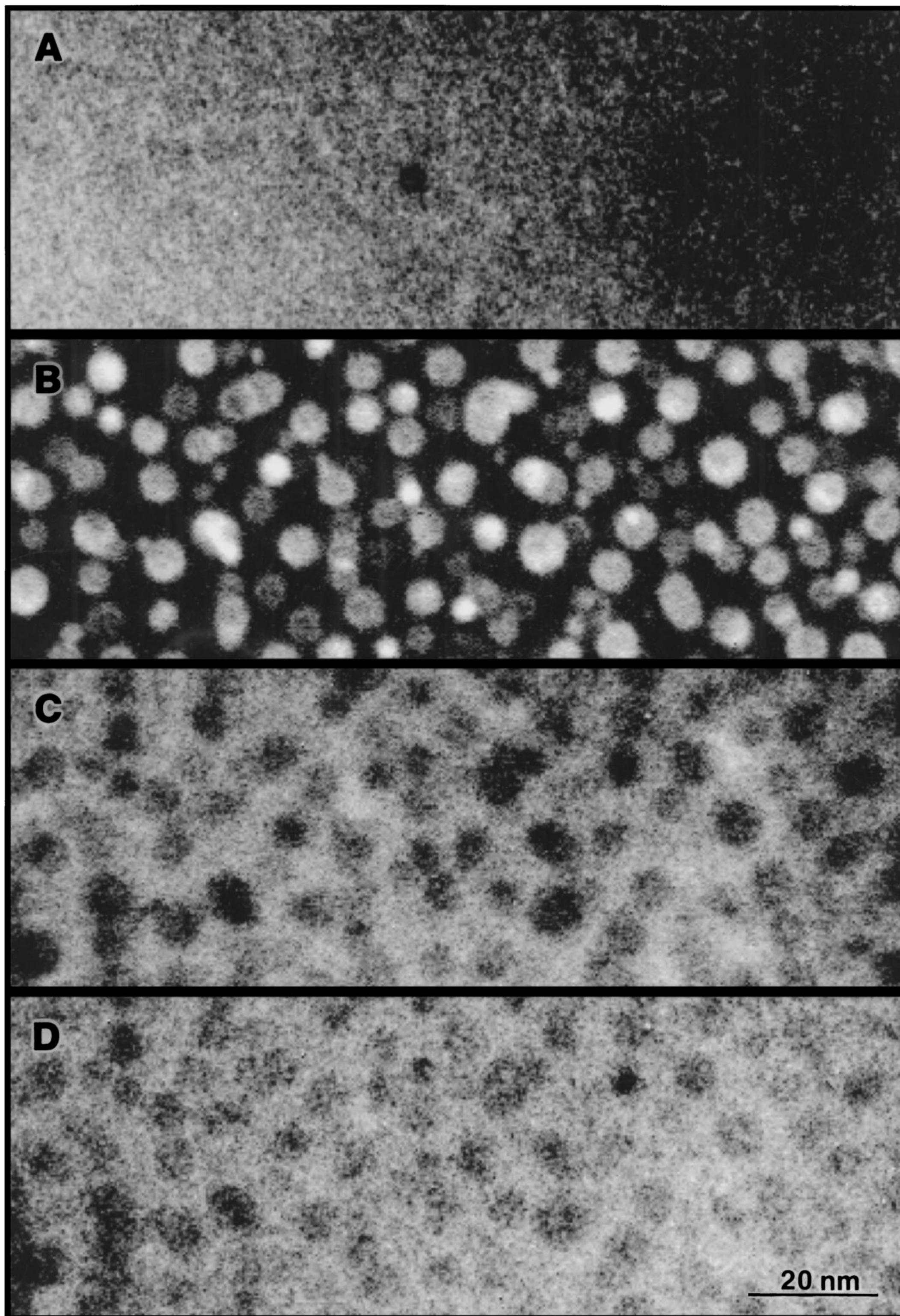

Figure 9 Series of EFTEM images from the 77 K Y^+-implant into alumina. Image A) is a bright field image, B) is a 15 eV-loss image, C) is a 25 eV-loss image and D) is a 40 eV-loss image.

theoretically predicted maximum values. This shows that it is possible for the reported doses of implanted ions to produce the amount of free Al required to form the particles imaged in these substrates, consistent with the proposed mechanism. Initially, it appears that these experimental volume fractions may be consistently under-estimated due to the assumptions made in the calculations. In particular, the thickness of the layer in which the implanted ions and/or particles reside is uncertain. This thickness of the particle-bearing material cannot be measured without imaging the implants in cross section, which proved to be problematic for these substrates. Both the theoretical and experimental volume fractions use the projected range (R_P) of the implanted ions as the relevant thickness in the total volume calculation. It is not reasonably expected that the particles would reside in a region thicker than this range because the concentration of the implanted ion is very low outside this region. It is possible, however, that the particles are present over a smaller thickness. If

TABLE I Comparison of theoretical and experimental aluminum volume fraction

Implant Conditions	VF_T, theoretical volume fraction (%)	VF_{ED}, experimental volume fraction (%)
150 keV, 5×10^{16} Y^+/cm^2, 298 K	14.9	7.5
130 keV, 5×10^{16} Y^+/cm^2, 298 K	15.8	7.8
150 keV, 2.5×10^{16} Y^+/cm^2, 298 K	8.2	4.8
150 keV, 5×10^{16} Y^+/cm^2, 873 K	14.9	11.4
150 keV, 5×10^{16} Y^+/cm^2, 77 K	14.9	1
50 keV, 5×10^{16} Ca^+/cm^2, 298 K	16.6	5.1

the thickness of the particle bearing region is reduced the experimentally measured volume fraction value increases. The same situation occurs if the full thickness of the particle-bearing material is not contained in the region of the TEM foil imaged. The first source of error can not be investigated without examination of a cross sectional sample. However, efforts were made in the imaging and measurement process to take particle measurements from regions of the sample that exhibited the greatest visible particle density. This precaution ensures that the whole particle range is contained in the section of the thin foil represented in the image. The fact that the average TEM thin foil thickness is approximately twice as thick as the maximum range for any of the implantations studied here is additional assurance that this source of error has been minimized. With these stated considerations, it appears that the comparison of theoretical and experimental volume fractions indicates that the implanted ions are capable of producing the volume of Al imaged in these substrates.

The implantations carried out at different temperatures should have the same retained dose and approximately the same concentration profile of implanted ions; however their different thermal histories give rise to different amounts of Al in the detected particles. The implantation carried out at 77 K should contain a smaller volume of metallic aluminum particles based on the restricted amount of thermal energy available for particle formation as compared with a similar room temperature implant. This assumption was supported by the peak intensities seen in the optical absorption spectra for these samples. It is also supported by the much lower experimental volume fraction. Conversely, the 873 K implantation should contain a larger volume of Al in particle form due to the greater amount of thermal energy available for diffusion during the implantation. Again, the optical absorption peak intensities support this conclusion, as does the experimental volume fraction calculation

In conclusion, the assumptions inherent in the experimental estimation of the volume fraction can introduce a significant error. However, the most problematic assumption concerns the volume of material containing the Al particles. This estimate could cause the greatest amount of error; however, it was used for both the theoretical and experimental calculations. This makes the absolute volume fraction uncertain, but it allows a confident comparison of the two calculations. The fact that the experimental volume fractions are, in every case smaller than the theoretical maximum volume fractions indicates that the reduction of the substrate by the implanted ion in each case would be more than sufficient to supply the Al that is imaged in each substrate in the form of particles. In addition, those implantations carried out under special conditions and expected to have varied volume fractions follow the expected trends very well.

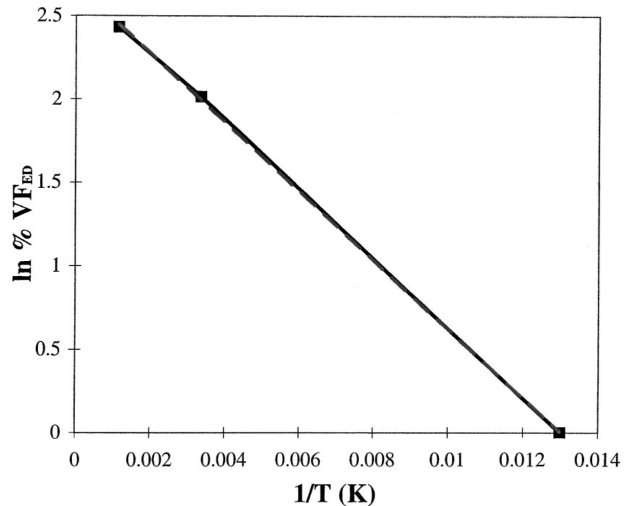

Figure 10 Arrhenius-type plot of ln(% VF_{ED}) vs. 1/T showing the linear temperature dependence of the Al volume fraction measured from the temperature controlled series of Y^+-implantations.

3.5. Dependence of volume fraction on implantation temperature

An examination of the temperature dependence of the volume fraction values (VF_{ED}) as a function of implantation temperature sheds light on the kinetics of the particle formation process discussed earlier. All of the implantations in the varied temperature series were carried out at the same incident ion energy, to the same incident ion dose and at the same approximate current density; therefore, the implantations took approximately the same amount of time. Therefore, the volume fraction estimates may be viewed to a first approximation as an Al particle formation rate. When the natural log of a temperature dependent rate is plotted versus the inverse of the temperature at which the process took place, an activation energy may be determined from the resulting line if the trend is linear (Arrhenius-dependent). This analysis was carried out using the experimental volume fraction data (VF_{ED}) from the substrates implanted at 873, 298 and 77 K and the resulting plot and its linear trendline are shown in Fig. 10. The activation energy (Q) determined from the slope is quite low at 1.7 kJ/mole. Typical activation energies for the diffusion of Al^+ in polycrystalline and single crystalline alumina range from ~110 kJ/mole to more than 650 kJ/mole [26–29]. However, the effects of irradiation can significantly enhance diffusion in these types of materials by lowering the diffusion activation energy during the implantation, as will be discussed.

4. Summary and discussion

The importance of the energy that is incident on, and present in the substrate during Y^+ implantation to the formation of Al particles has been demonstrated through a series of implantations in which both the incident ion energy and the thermal energy were controlled, see Fig. 4. The roles of both types of energy have been determined by the analysis of experimental data and it has been shown that both are critical to the formation of Al particles in reduced alumina substrates.

The highest temperature and energy implantations resulted in the formation of crystalline aluminum particles. The particles were slightly larger in the higher incident ion energy implants and significantly larger in the high thermal energy implantation. This large particle size is the result of the greater thermal energy available for the diffusion of the free Al that is produced by reduction of the substrate. This behavior is consistent with the expected thermal dependence of atom mobility in solids. The lower temperature implantations appear to be inconsistent with this trend as they show that the atom mobility appears to be significant even at lower temperatures (77 K) than traditionally expected. When the Arrhenius relationship between the experimentally measured particle volume fraction and the implantation temperature is examined, an activation energy of $\sim$2 kJ/mole (406 cal/mole) is calculated. This activation energy is significantly lower than that expected for Al diffusion in alumina.

The lower incident ion energy implantation experiments (100 keV and 60 keV) that were carried out at room temperature produced predominantly amorphous Al clusters and no Al clustering, respectively. This result is inconsistent with the assumption that Al particle formation relies solely on the presence of sufficient thermal energy for diffusion of the free Al atoms. Based on the results of the other room temperature implantations, there appears to be enough thermal energy available in both low incident energy experiments for crystalline particle formation, however, no such particles are detected. These results indicate that there is an important, incident energy dependent factor aside from the thermal energy that affects the particle formation in these substrates. The exact effect of the incident energy on the deposited energy in the substrate is difficult to determine due to sputtering of the surface material during implantation. It would be expected that lower energy ions would result in both ion and energy deposition profiles that are narrower and closer to the substrate surface than their higher energy counterparts. However, when surface sputtering is taken into account the ion profiles of high and low energy implants are surprisingly similar, with nearly equal concentrations and depths. This effect is due to the higher sputtering coefficient for the lower energy ions. The changing sputtering coefficient also affects the deposited energy profile for the lower energy ions. Much of the material that absorbs implanted ion energy will be sputtered away by the time the implantation is complete and that material is not taken into account when finding the final thickness (depth) of the implanted material. This effect makes the low energy calculations of the energy deposited per ion per unit length significantly higher than they are in reality. Because of the complexity of precisely determining these values and the misleading nature of the raw calculations they are not discussed in relation to particle formation here except to note that an important role is clearly played by the incident ion energy.

The importance of the fluence of the incident (reducing) ion was also shown to play a role in particle formation, (Fig. 2). It has been shown that the implantation of 5×10^{16} Y^+/cm^2 results in the formation of crystalline particles. The implantation of half of this fluence also results in crystalline particles. The implantation of 1×10^{16} Y^+/cm^2 is insufficient for particle formation. It is possible that there is a minimum threshold concentration of Y^+ ions or Al atoms that is necessary for particle formation; however, it is also possible that the same incident energy dependent factor mentioned above is responsible for the lack of particle formation in this low fluence sample. The actual incident ion energy is the same (150 keV) as the other, particle forming implantations; however, the total energy dose incident on the substrate is smaller due to the much lower ion fluence. This difference in total energy dose deposited in the substrate may explain the lack of particle formation at this low ion fluence.

It is proposed that the critically important, incident/deposited energy dependent mechanism that appears to be responsible for the apparently inconsistent results summarized above is radiation enhanced diffusion (RED) caused by the ion implantation treatments. RED allows the activation energy for atomic diffusion in a solid to be significantly reduced during ion implantation. For example, Arnold *et al.* [32] and Mazzoldi [30] have shown that Rb diffusion in Rb_2O-SiO_2 glass can have activation energies ranging from 1–4 kJ/mole during heavy ion irradiation. This range is comparable with the calculated activation energy of 1.7 kJ/mole for the Al particle formation process studied here. The presence of RED during implantation would also explain the formation of Al particles even at temperatures significantly below the limit where "normal" diffusion processes become insignificant due to reduced thermal energy. The occurrence of a significant amount of diffusion below room temp is characteristic of RED [31], which is only heavily dependant on temperature above $\sim$298 K [32]. Pivin and Colombo have seen definite evidence of RED at temperatures as low as 100 K and suspect that it occurs at lower temperatures, but were unable to detect the very small particles that would result using X-ray diffraction. At temperatures as low as 44 K it is possible that even RED is suppressed due to either the very low defect mobility and/or the temperature dependence of particle nucleation. If RED is still active at this temperature, the volume fraction of particles formed, according to the calculated activation energy is so small as to be undetectable ($\sim$0.1%).

Lastly, the presence of RED in this system also explains the lack of particle formation in both the 60 keV and 1×10^{16} ions/cm^2 implantations. The 60 keV implanted substrate was subjected to a large fluence of low energy ions, while the other underwent irradiation with

a small fluence of high energy ions. It appears that neither implanted substrate experiences the effects of radiation enhanced diffusion and therefore the "normal" activation energy of Al in alumina would apply in these circumstances. The magnitude of this ordinary activation energy (100–650 kJ/mole) would prevent the diffusion required for Al particle formation during a room temperature implantation. The 60 keV sample may not experience particle formation as a result of a reduced defect concentration, an important factor in RED. The low fluence implanted substrate was exposed to ions with sufficient energy to produce defects, but the small magnitude of the implant may shorten the implant time sufficiently to prevent particle formation at room temperature.

In conclusion, there are three mechanisms responsible for the formation of Al particles in alumina substrates implanted at moderate temperatures. First, reduction of the substrate by the implanted ion must take place. Thermodynamic calculations show that this reaction is possible for the $Y + Al_2O_3$ system. It is assumed that the reaction goes to completion in all implanted substrates and experimental evidence from many of the substrates has shown that is does occur. Second, the activation energy for the diffusion of Al in the substrate is lowered by the effects of RED; and third, there must be sufficient thermal energy to overcome that lowered activation energy and cause Al diffusion.

Acknowledgments

This work has been partially supported by the National Science Foundation under Grant No. DMR-9624927. The authors wish to acknowledge the assistance and support rendered by Dr. N. D. Evans and Dr. D. B. Poker, at the Oak Ridge Institute for Science and Technology and the Oak Ridge National Laboratory, respectively. The support of the SHARE Program under contract DE-AC05-76OR00033 with Oak Ridge Associated Universities and that of the U.S. Department of Energy, under contract DE-AC05-96OR22464 with Lockheed Martin Energy Research Corp. is acknowledged.

References

1. C. W. WHITE, D. S. ZHOU, J. D. BUDAI, R. A. ZUHR, R. H. MAGRUDER and D. H. OSBORNE, *Mat. Res. Soc. Symp. Proc.* **316** (1994) 499.
2. A. P. MOURITZ, D. K. SOOD, D. H. ST. JOHN, M. V. McSWAIN and S. J. WILLIAMS, *Nuc. Inst. and Meth. B* **B19/20** (1987) 805.
3. R. F. HAGLUND JR., L. YANG, R. H. MAGRUDER, C. W. WHITE, R. A. ZUHR, L. YANG, R. DORSINVILLE and R. R. ALFANO, *ibid.* **91** (1994) 493.
4. J. ALLEGRE, G. ARNAUD, H. MATHIEU, P. LEFEBVRE, W. GRANIER and L. BONDES, *J. Crys. Growth* **138** (1994) 998.
5. F. L. FREIRE, N. BROLL and G. MARIOTTO, *Mat. Res. Soc. Symp. Proc.* **396** (1996) 385.
6. L. ROMANA, P. THEVENARD, B. CANUT, G. MASSOURAS, R. BRENIER and M. BRUNEL, *Nuc. Inst. and Meth. B* **B46** (1990) 94.
7. P. S. SKLAD, C. J. McHARGUE, C. W. WHITE and G. C. FARLOW, *J. Mater. Sci.* **27**(21) (1992) 5895.
8. C. J. McHARGUE, S. REN, P. S. SKLAD, L. F. ALLARD and J. HUNN, *Nuc. Inst. and Meth. B* **B116** (1996) 173.
9. M. OHKUBO and N. SUZUKI, *Phil. Mag. Lett.* **57**(5) (1988) 261.
10. C. W. WHITE, J. D. BUDAI, S. P WITHROW, S. J. PENNYCOOK, D. M. HEMBREE, D. S. ZHOU, T. VO-DIHN and R. H. MAGRUDER, *Mat. Res. Soc. Symp. Proc.* **316** (1994) 487.
11. E. M. HUNT and J. M. HAMPIKIAN, *J. Mater. Sci.* **32** (1997) 3393.
12. *Idem.*, *Acta Materialia* **47**(5) (1999) 1497.
13. A. E. HUGHES, *Rad. Eff.* **74** (1983) 57.
14. A. B. SCOTT, W. A. SMITH and M. A. THOMPSON, *J. Physical Chem.* **57** (1953) 757.
15. N. G. POLITOV and L. F. VOROZHEIKINA, *Sov. Phys.-Solid State.* **12** (1970) 237.
16. P. VAJDA and F. BEUNEU, *Nuc. Inst. and Meth. B* **116** (1996) 183.
17. B. D. EVANS and M. STAPELBROEK, *Phys. Rev. B* **18**(12) (1978) 7089.
18. T. SHIKAMA and G. P. PELLS, *Phil. Mag. A* **47**(3) (1983) 369.
19. J. M. BUNCH, J. G. HOFFMAN and A. H. ZELTMANN, *J. Nuc. Mat.* **73** (1978) 65.
20. E. M. HUNT, J. M. HAMPIKIAN, D. B. POKER and N. D. EVANS, *Surface and Coatings Technology* **103/104** (1998) 409.
21. E. M. HUNT, J. M. HAMPIKIAN and N. D. EVANS, in "Microscopy and Microanalysis" edited by G. W. Bailey *et al.*, (Minneapolis, MN, 1996) p. 534.
22. E. M. HUNT, Z. L. WANG, N. D. EVANS and J. M. HAMPIKIAN, in "Microscopy and Microanalysis" (Minneapolis, MN, 1997).
23. *Idem.*, *Micron.* **29**(2/3) (1998) 191.
24. PROFILE Ion Implantation Code, Implant Sciences Corp., 35 Cherry Hill Drive, Danvers MA 09123, (508) 777-5110.
25. E. M. HUNT, Ph.D. Thesis, Georgia Institute of Technology, 1998.
26. P. KOFSTAD, "High Temperature Corrosion," (Elsevier Applied Science, New York, 1988) Chapter 4.
27. M. W. BRUMM and H. J. GRABKE, *Corrosion Science* **33**(11) (1992) 1677.
28. K. MAKI, M. SHIODA, M. SAYASHI, T. SHIMIZU and S. ISOBE, *Materials Science and Engineering* **A153** (1992) 591.
29. P. MAZZOLDI and A. MIOTELLO, *ibid.* **A115** (1989) 1.
30. G. ARNOLD, G. BATTAGLIN, G. DELLA MEA, G. DEMARCHI, P. MAZZOLDI and A. MIOTELLO, *Nuc. Inst. and Meth. B* **32** (1998) 315.
31. J. C. PIVIN and P. COLOMBO, *ibid.* **122** (1997) 522.
32. K. NEUBECK, H. HAHN, A. G. BALOGH, H. BAUMANN, K. BETHGE, D. M. RUECK and N. ANGERT, *J. of Mater Res.* **11** (1996) 1277.
33. P. J. BURNETT and T. F. PAGE, *J. Mater. Sci.* **19** (1984) 3524.
34. C. W. WHITE, L. A. BOATNER, P. S. SKLAD, C. J. McHARGUE, J. RANKIN, G. C. FARLOW and M. J. AZIZ, *Nuc. Inst. and Meth. B* **B32** (1988) 11.
35. A. TSUGE, K. MIZUNO, T. UNO and K. TATSUMI, *Nippon Kizoku Gakkaishi* **59** (1995) 1095.

Received 2 March
and accepted 3 August 2000